Available online at www.sciencedirect.com
SCIENCE DIRECT®
Physics of the Earth and Planetary Interiors 146 (2004) 469–481
PHYSICS OF THE EARTH AND PLANETARY INTERIORS
www.elsevier.com/locate/pepi

Some comments on the effects of lower-mantle anisotropy on SKS and SKKS phases

Stéphen A. Hall[1], J.-M. Kendall*, Mirko van der Baan

School of Earth Sciences, University of Leeds, Leeds, LS2 9JT, UK

Received 1 September 2003; received in revised form 10 May 2004; accepted 11 May 2004

Abstract

Anisotropy in the lowermost few 100 km of mantle, or D″ region, is indicative of deformation-induced alignment of crystals and/or inclusions of material, and as such offers insights into the dynamic nature of this region. Observations of shear-wave splitting in phases that transit this region provide constraints on such anisotropy. We investigate the effects of lower-mantle seismic anisotropy on SKS and SKKS phases through linked effective-medium modelling and ray-based waveform modelling. A mantle with vertical-transverse-isotropy (VTI) will not produce any splitting in such core phases. Instead we consider the effects of azimuthal-anisotropy due to aligned disk-shaped and tubular inclusions and aligned perovskite, periclase and columbite. Models are constructed subject to constraints imposed by observed anisotropy (<3%) and plausible variations in aggregate isotropic velocities (< ± 2.5%). Melt-filled inclusions are much more effective in generating anisotropy than solid-filled inclusions and disk-shaped inclusions produce more anisotropy than tubular inclusions. In general the degree of splitting produced by most of the models is small, similar to that produced by the crust (<0.5 s). The exceptions are melt-filled vertically-aligned disk-shaped inclusions and horizontally aligned periclase, the former most likely in low-velocity regions, the latter in high-velocity regions. Both models produce splitting significant enough to mask the effects of upper-mantle anisotropy. Strong azimuthal variations in splitting and discrepancies in SKS and SKKS splitting are diagnostic of these anisotropic models.

Keywords: Anisotropy; D″; Seismology; Core phases; Composition of the Earth

1. Introduction

The interpretation of seismic anisotropy in the deep Earth provides insights into mineralogy, composition and dynamic processes. As seismologists find increasing evidence for anisotropy in most parts of the solid Earth, one of the challenges facing such analyses is constraining the anisotropy to a particular region. Here, we investigate the effects of anisotropy in the lowermost mantle, or D″ region, on the seismic phases SKS and SKKS (Fig. 1). These phases are more commonly used to investigate upper-mantle anisotropy (e.g., Silver, 1996; Savage, 1999), and the effects of anisotropy in deeper parts of the Earth are generally neglected.

Interpretations of D″ anisotropy are normally based on evidence of shear-wave splitting in phases which turn near or diffract along the core–mantle boundary (CMB). Such observations show regional variations

* Corresponding author.
E-mail addresses: steve.hall@pet.hw.ac.uk (S.A. Hall), m.kendall@earth.leeds.ac.uk (J.-M. Kendall), mirko@earth.leeds.ac.uk (M. van der Baan).
[1] Present address: Laboratoire 3S, UJF-INPG-CNRS, Grenoble Cedex 9, France.

0031-9201/$ – see front matter © 2004 Published by Elsevier B.V.
doi:10.1016/j.pepi.2004.05.002

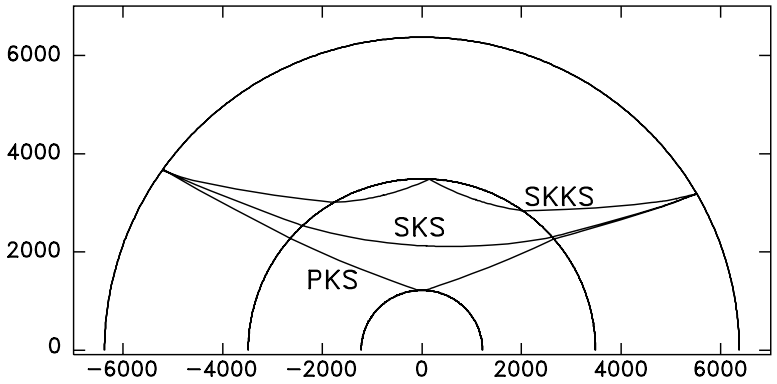

Fig. 1. Example raypaths for the core phases SKS, SKKS and PKS. Units are in kilometers.

and suggest differences between regions of upwelling and downwelling (see reviews in Lay et al., 1998; Kendall and Silver, 1998). Anisotropy in the D″ region has been attributed to the lattice preferred alignment (LPO) of minerals, the preferred alignment of small-scale inclusions or the layering of contrasting materials (Kendall and Silver, 1998; Karato, 1998; Yamazaki and Karato, 2002). The latter two categories are often referred to as shape-preferred-orientation (SPO).

In 1D isotropic Earth models, a P-wave in the liquid outer-core converts to a vertically polarized shear-wave (SV-wave) at the CMB and is thus not recorded on the transverse-component of a seismometer at the Earth's surface. However, the presence of transverse-component energy is often observed and is indeed an indication that the shear-wave (e.g., SKS) may have travelled through an anisotropic region along its path from the CMB to the Earth's surface.

A common class of anisotropy is vertical-transverse-isotropy (VTI), which is characterised by a lack of azimuthal variation in velocity within the horizontal plane. This refers to hexagonal symmetry with a vertical symmetry axis and synonyms include polar or radial anisotropy. This style of anisotropy can be produced by fine-scale horizontal layering or the preferred alignment of tabular inclusions in the horizontal plane. It can also be caused by crystal alignment, for example, the vertical alignment of a particular crystal axis with a random azimuthal orientation of the other crystal axes. The preferred alignment of olivine a-axes in the horizontal plane, but not in any azimuthal direction (i.e., a global average), is the cause of VTI anisotropy in the uppermost mantle of the Earth model PREM (Dziewonski and Anderson, 1981).

It is important to note that, as with the isotropic case, VTI anisotropy will not produce any SKS (SKKS, PKS) transverse-component energy as the P–SV-wave system is mathematically decoupled from that for SH-waves (Aki and Richards, 1980). The core-transiting P-wave will only transmit a P- and SV-wave when entering the mantle. In other words, SKS and SKKS will not produce any shear-wave splitting in a VTI mantle, regardless of epicentral distance. Shear-wave splitting in such core phases is produced by a more general form of anisotropy. Here, we use the term azimuthal anisotropy to refer to a style of anisotropy where there are azimuthal variations in velocities within the horizontal plane.

Discrepancies are sometimes observed in shear-wave splitting in SKS and SKKS phases for a given source and station (James and Assumpção, 1996). The phases SKS and SKKS travel similar raypaths through the upper mantle but are nearly 1000 km apart at the CMB (Fig. 1). Such discrepancies can be therefore attributed to lower-mantle effects, such as: CMB boundary topography (Restivo et al., 1998), significant lateral velocity gradients or azimuthal anisotropy. Here, we investigate SKS and SKKS sensitivity to a variety of plausible forms of azimuthal anisotropy using constraints from current seismic observations. Effective-medium modelling and Voigt–Reuss–Hill (VRH) averaging are used to determine the elasticity and anisotropy in D″ due to potential SPO and LPO

fabrics. This modelling allows the determination of transmission coefficients and shear-wave splitting for SKS and SKKS phases.

2. Elastic properties of possible SPO and LPO fabrics in D″

A number of different plausible models have been suggested to explain lower-mantle anisotropy. Firstly, D″ anisotropy could be caused by SPO fabric due to the alignment of ellipsoidal inclusions within an isotropic matrix. These inclusions could be solid or melt-filled and either disk-shaped (aspect ratio $\ll 1$) or tubular (aspect ratio $\gg 1$) (Kendall and Silver, 1998). Hence, four different SPO models are considered in our numerical simulations. The elastic properties of these aligned inclusions are obtained using the effective-medium approach of Tandon and Weng (1984). Use of effective-medium theories explicitly assumes that the inclusions are much smaller than the characteristic wavelengths of the seismic phases and that frequency-dependent scattering effects can be neglected.

Alternatively, anisotropy in D″ could be caused by the alignment of anisotropic minerals, such as perovskite, yielding an LPO fabric. Alignment of mineral grains due to flow, can produce both azimuthal anisotropy or a VTI symmetry. Slip-planes of minerals align parallel to the flow plane. If the slip directions are randomly oriented within a horizontal slip plane then the resultant medium displays VTI symmetry (Stixrude, 1998). However, with most minerals (e.g., olivine) an LPO is generated in a slip direction parallel to the flow direction thus generating an azimuthally anisotropic medium. Partial development of the fabric results in a limited degree of anisotropy. Hence, alignment of minerals which are inherently anisotropic will usually lead to azimuthal anisotropy in the aggregate material. The elastic coefficients of such an aggregate medium can be determined using Voigt–Reuss–Hill averaging (Hill, 1952; Anderson, 1965).

The overall seismic properties of the lowermost mantle and its isotropic P- and S-wave velocities are constrained from from both global and regional studies. Therefore, any modelling of the LPO or SPO fabrics must fit within these known limits. The seismic constraints we use are that the maximum horizontal shear-wave anisotropy must be less than 3% and that the deviation from the observed isotropic velocities is less than 2.5%.

Although the term percentage of anisotropy is poorly defined in the literature, with respect to the lower mantle the stated values of 2–3% generally refer to the degree of shear-wave splitting observed in horizontally propagating (i.e., turning) shear-waves in the D″ region (Kendall and Silver, 1998). Therefore, the percentage anisotropy is defined as

$$\%\,\text{anisotropy} = 200\left(\frac{v_{s_1} - v_{s_2}}{v_{s_1} + v_{s_2}}\right), \tag{1}$$

with v_{s_1} and v_{s_2} the velocities of the fast, S_1, and slow, S_2, shear waves for a particular azimuth of horizontal wave propagation.

Fig. 2 illustrates the seven different models used to examine the potential effects of azimuthal anisotropy (i.e., non-VTI) in D″ on splitting measurements of SKS and SKKS phases. In each case the volume-fraction of aligned inclusions (for SPO media) and degree of alignment (for LPO media) is such that the horizontal shear-wave anisotropy is maximised (but less than 3%) while retaining aggregate isotropic properties which deviate by less than 2.5% from the given physical parameters. The starting isotropic model is outlined in Fig. 3. For the four SPO models, the inclusions are embedded in a matrix with standard lower mantle properties with an orientation that produces azimuthal anisotropy (hexagonal symmetry with a horizontal symmetry axis). The symmetry axis is aligned along x_1. The three LPO models considered are a weighted VRH average of known isotropic lower-mantle properties and the properties of aligned perovskite (orthorhombic), periclase (cubic) or columbite (orthorhombic) (see Fig. 2). The elastic constants of the aligning minerals are taken from Stixrude (1998) who determined them numerically for lower-mantle pressure conditions, but at absolute-zero temperature. Perovskite elasticities have been calculated for lower-mantle pressures and temperatures (Oganov et al., 2001), but we have yet to test the temperature effects in our modelling. The symmetry of the assemblages are rotated to respectively align the slip-plane and slip-direction parallel to a horizontal flow-plane and flow along x_1 (Stixrude, 1998).

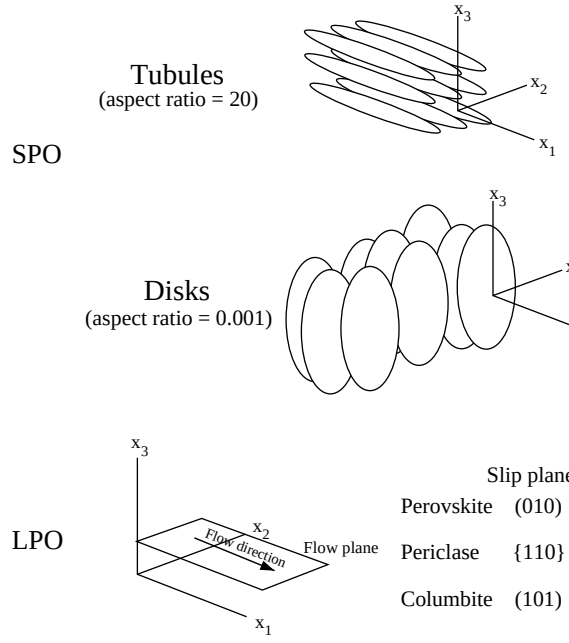

Fig. 2. Possible mechanisms for azimuthal anisotropy in D″ used in the numerical modelling. Model parameters are chosen to be consistent with seismic observations (i.e., anisotropy <3% and changes in isotropic aggregate velocities < ± 2.5%). Vol. Frac. is the percentage volume occupied by inclusions; %Anis. is the degree of shear-wave anisotropy (equation 1); Vp-dev. and Vs-dev. indicate the percentage deviation of the VRH-average model velocities from the known lower-mantle values.

If the anisotropy is caused by aligned ellipsoidal inclusions (SPO), melt-filled inclusions provide a more effective mechanism for inducing anisotropy than solid-filled inclusions, without causing large deviations in the bulk-average seismic velocities (see table in Fig. 2). Note the small quantities of melt needed to produce a large percentage of anisotropy. Tubules (cigar-shaped inclusions) are less effective

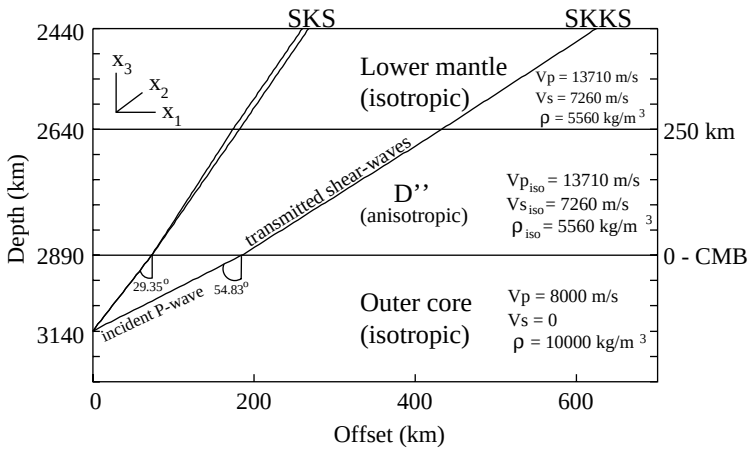

Fig. 3. Model used for ray tracing, which is in turn used to determine CMB transmission coefficients and shear-wave splitting parameters. Raypaths for SKS and SKKS phases that travel to an epicentral distance of 110° are also shown.

in generating anisotropy than disks (penny-shaped inclusions). Partial alignment of perovskite and periclase minerals (LPO) quickly causes significant anisotropy without introducing large deviations from bulk-average isotropic velocities, presumably because the lower mantle is primarily comprised of perovskite and periclase. On the other hand, columbite is very high in seismic velocity and quickly introduces large increases. In order to limit the bulk increase in velocity to 2.5%, only small amounts of aligned columbite can be included, thereby reducing the amount of predicted anisotropy (Fig. 2).

3. Effects of azimuthal anisotropy in D″ on SKS and SKKS splitting

To examine the effect of azimuthal anisotropy on observations of SKS and SKKS phases within the mantle, azimuthal variations in transmission coef-

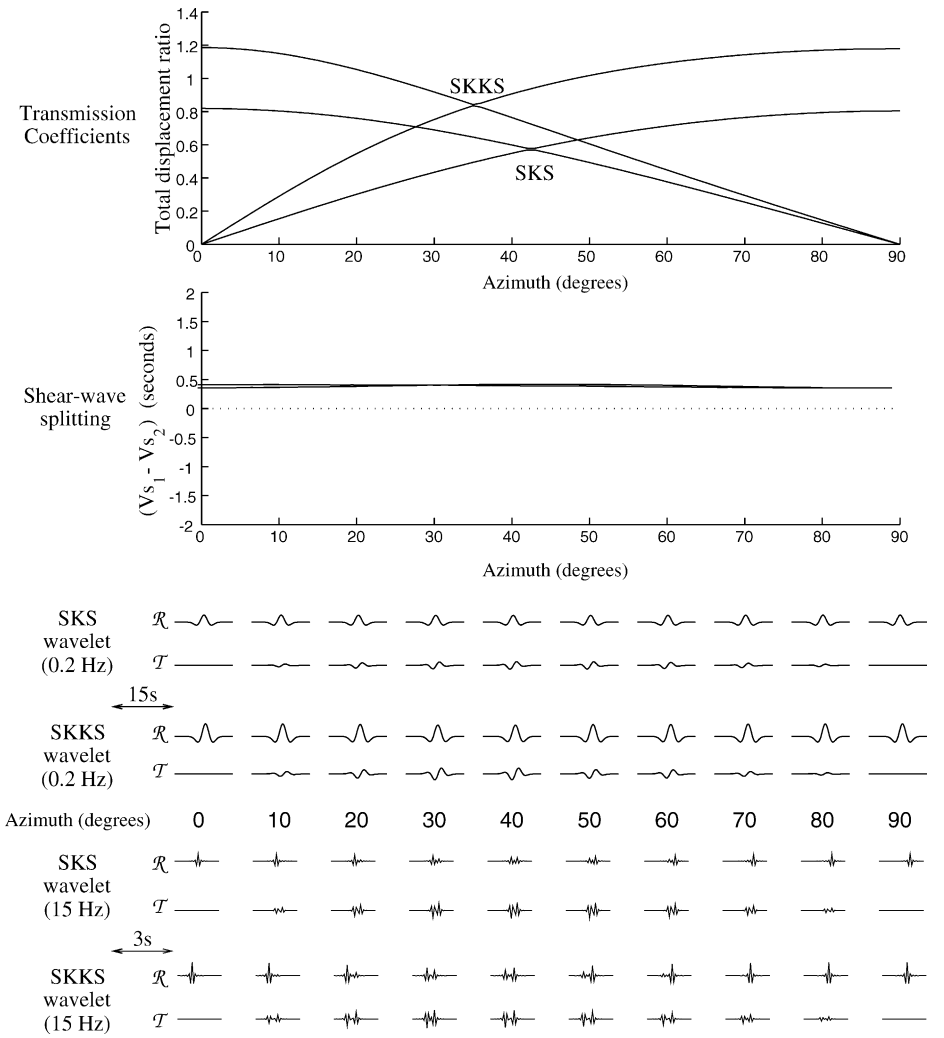

Fig. 4. D″ anisotropy due to aligned, melt-filled, tubular inclusions. Results are for SKS and SKKS phases at an epicentral distance of 110°. The figure (from top to bottom) shows azimuthal variations in transmission coefficients at the CMB, shear-wave splitting times, and the resulting radial (R) and transverse (T) component waveforms with 0.2 Hz and 15 Hz dominant frequencies. A time window of 15 s is shown for the 0.2 Hz waveforms and a shorter time window of 3 s is shown for the 15 Hz waveforms.

ficients, shear-wave splitting and synthetic waveforms are calculated for the 7 models described in Fig. 2. Transmission coefficients for a core transiting P-wave incident on the CMB are determined using the approach outlined in Guest and Kendall (1993). Transmission coefficients between an anisotropic solid/liquid interface are computed using expressions given in Mallick and Frazer (1991). The P-waves converted at the CMB are taken to have angles of incidence of 30° and 55° for SKS and SKKS, respectively, and correspond to an epicentral distance of roughly 110°. The azimuth is measured with respect to the x_1 direction (see Fig. 2). The transmission coefficient is given as the total displacement ratio of the transmitted wave amplitude to the incident wave. Shear-wave splitting, due to the D″ anisotropy, in SKS

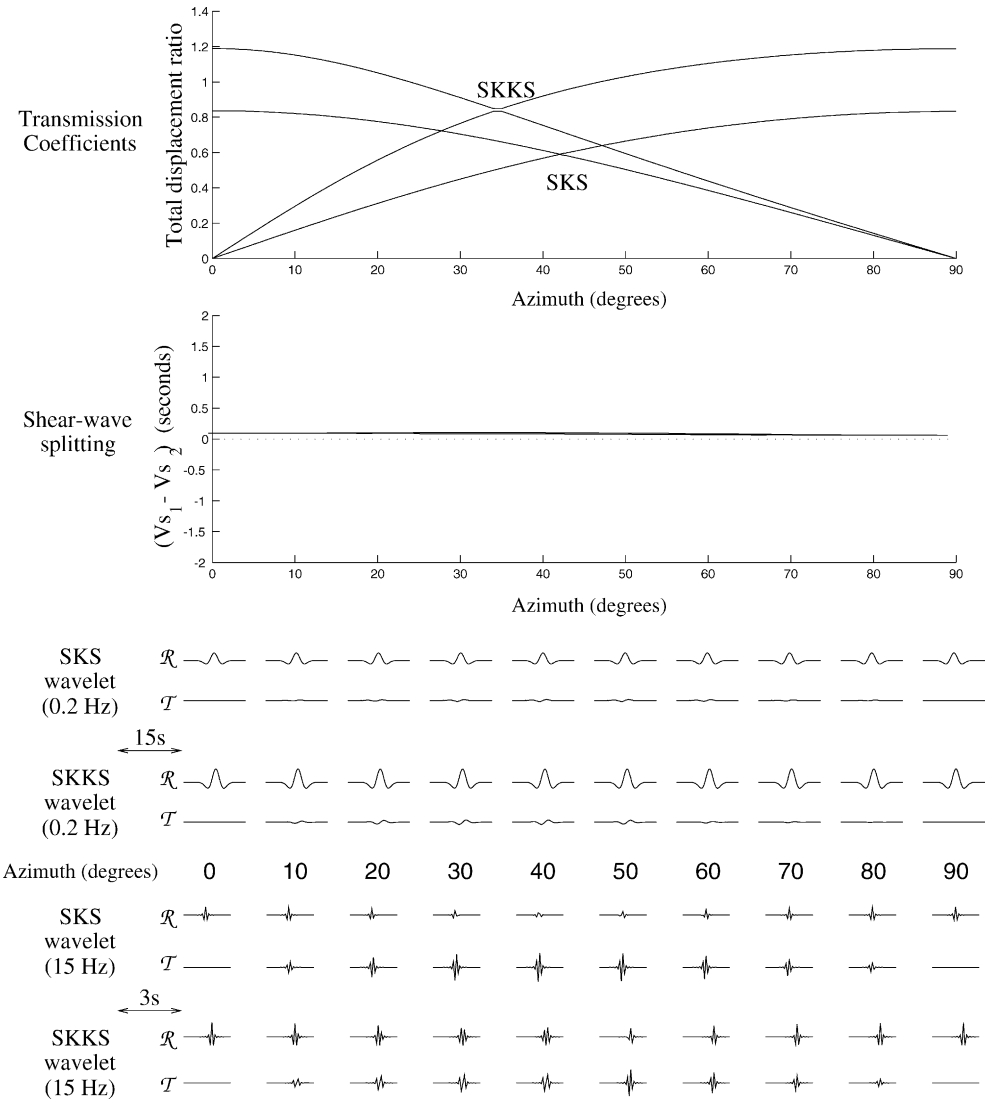

Fig. 5. D″ anisotropy due to aligned, solid, tubular inclusions. Results are for SKS and SKKS phases at an epicentral distance of 110°. The figure (from top to bottom) shows azimuthal variations in transmission coefficients at the CMB, shear-wave splitting times, and the resulting radial (R) and transverse (T) component waveforms with 0.2 Hz and 15 Hz dominant frequencies. A time window of 15 s is shown for the 0.2 Hz waveforms and a shorter time window of 3 s is shown for the 15 Hz waveforms.

and SKKS is also computed as a function of azimuth. Finally, radial and transverse components of synthetic waveforms are modelled by means of raytracing (Guest and Kendall, 1993). The synthetic data are convolved with Ricker wavelets of 0.2 Hz and 15 Hz, respectively. The 0.2 Hz wavelet represents a more realistic waveform for SKS and SKKS, whilst the 15 Hz wavelet provides a better indication of the energy distribution of the two shear-waves across the two components.

A number of factors influence whether or not appreciable shear-wave splitting is generated when an SKS or SKKS phase passes through the D″ region. The transmission coefficients at the CMB must be such that

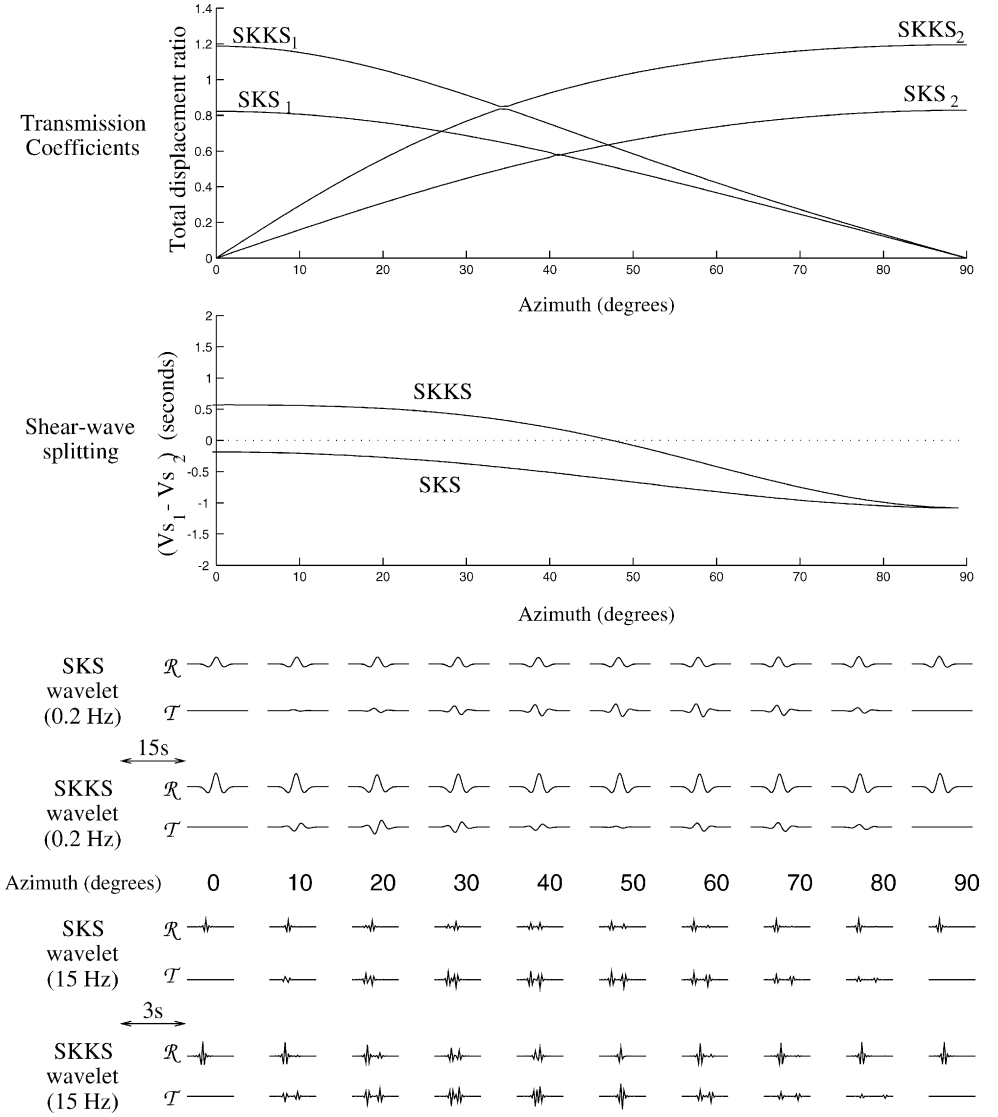

Fig. 6. D″ anisotropy due to aligned, melt-filled, disk-shaped inclusions. Results are for SKS and SKKS phases at an epicentral distance of 110°. The figure (from top to bottom) shows azimuthal variations in transmission coefficients at the CMB, shear-wave splitting times, and the resulting radial (R) and transverse (T) component waveforms with 0.2 Hz and 15 Hz dominant frequencies. A time window of 15 s is shown for the 0.2 Hz waveforms and a shorter time window of 3 s is shown for the 15 Hz waveforms.

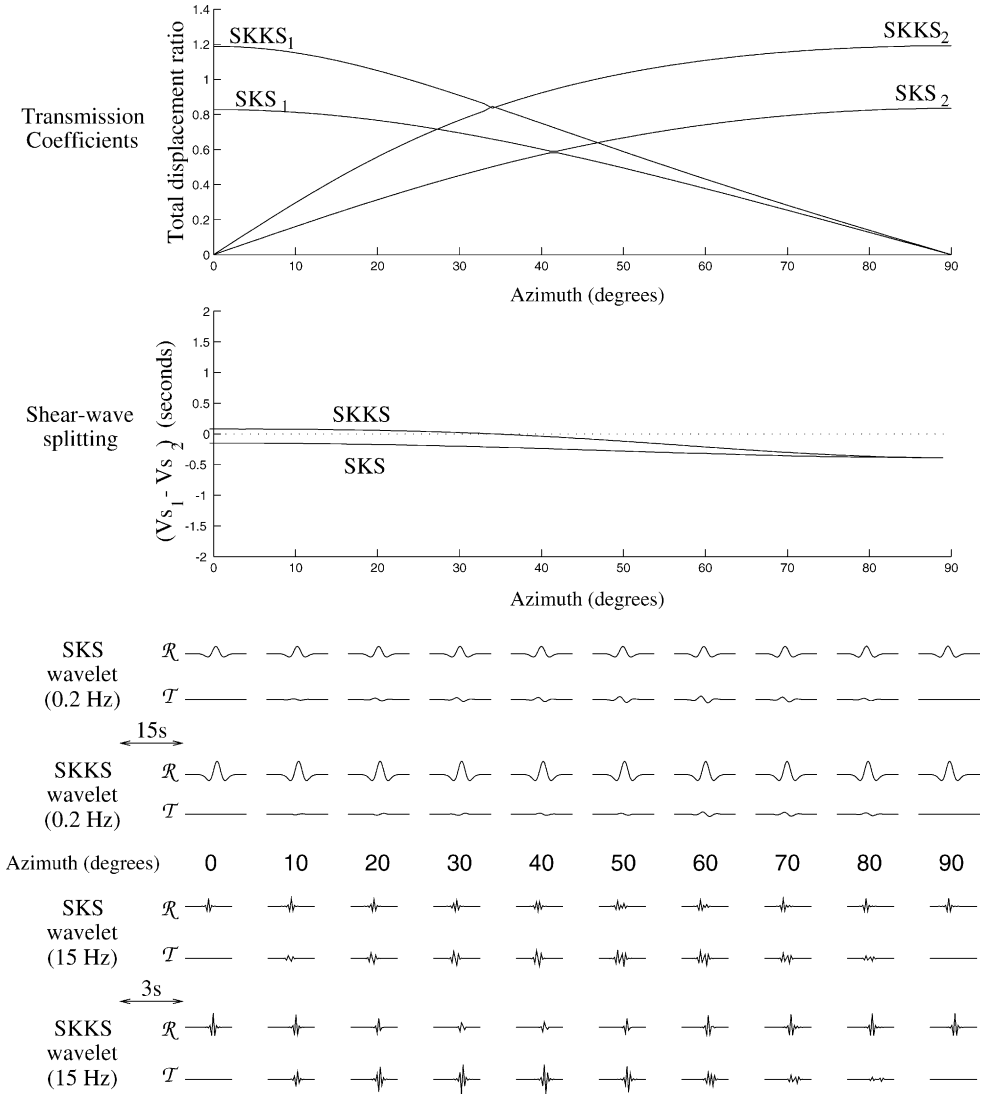

Fig. 7. D″ anisotropy due to aligned, solid, disk-shaped inclusions. Results are for SKS and SKKS phases at an epicentral distance of 110°. The figure (from top to bottom) shows azimuthal variations in transmission coefficients at the CMB, shear-wave splitting times, and the resulting radial (R) and transverse (T) component waveforms with 0.2 Hz and 15 Hz dominant frequencies. A time window of 15 s is shown for the 0.2 Hz waveforms and a shorter time window of 3 s is shown for the 15 Hz waveforms.

they effectively generate both fast and slow transmitted shear-waves. The anisotropy must be strong enough to generate resolvable splitting. Finally the transmitted shear-wave must be not aligned with a principle axes of the anisotropy.

The upper row in Figs. 4–10 displays the computed transmission coefficients for P-to-S conversion as a function of azimuth for both SKS and SKKS phases at 110°. With all 7 models (4 SPO and 3 LPO) two shear-waves are transmitted at azimuths away from the principle axes. These principle axes are the directions of propagation where the P–SV-waves are decoupled from the SH-phase and so no transverse (SH) energy is produced. For the SPO (Figs. 4–7) and perovskite (Fig. 8) models, these axes coincide with the coordinate axes (parallel and perpendicular to flow).

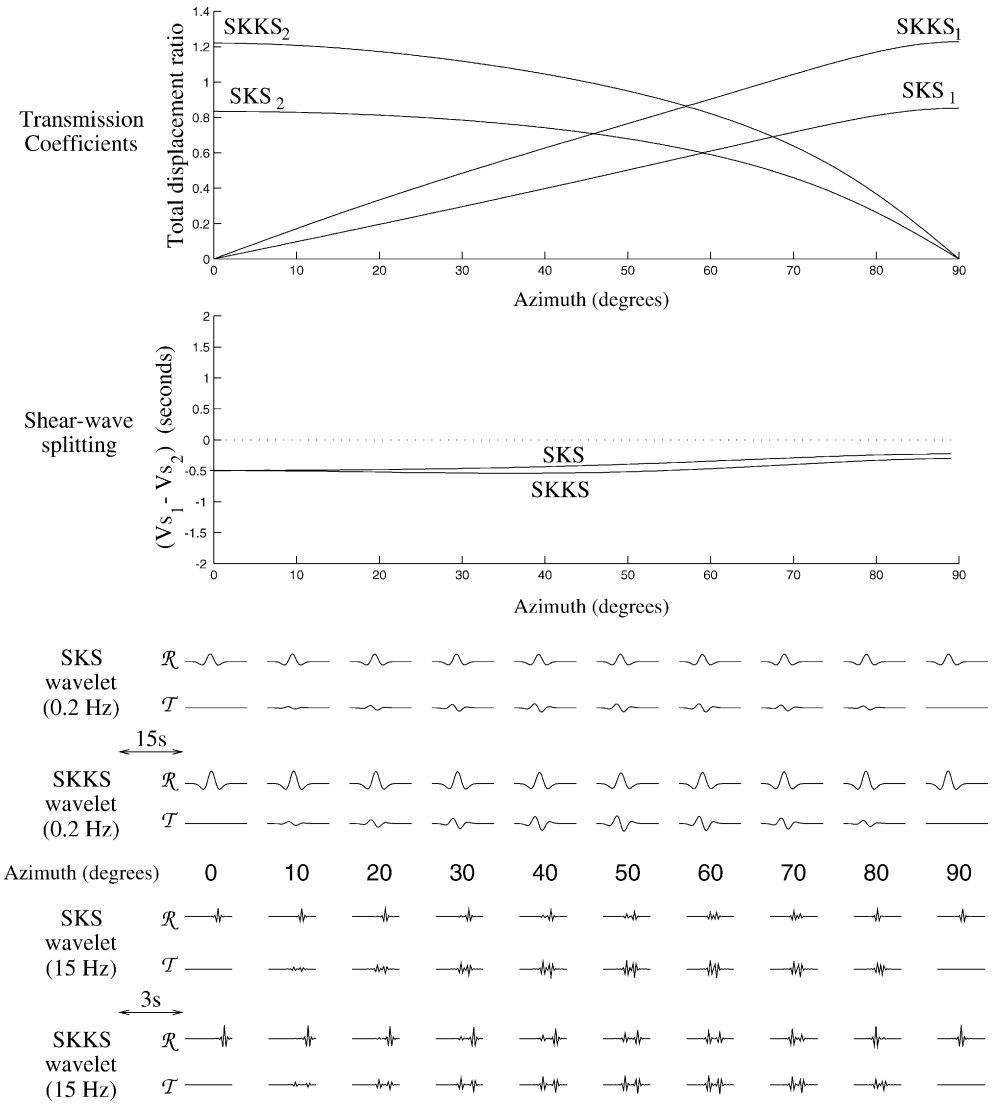

Fig. 8. D″ anisotropy due to partially aligned perovskite. Results are for SKS and SKKS phases at an epicentral distance of 110°. The figure (from top to bottom) shows azimuthal variations in transmission coefficients at the CMB, shear-wave splitting times, and the resulting radial (R) and transverse (T) component waveforms with 0.2 Hz and 15 Hz dominant frequencies. A time window of 15 s is shown for the 0.2 Hz waveforms and a shorter time window of 3 s is shown for the 15 Hz waveforms.

However, for periclase and columbite (Figs. 9 and 10) the principle axes are shifted from the coordinate axes since the orientation of the slip-planes and slip-directions are not along the principle axes of the mineral anisotropy. The principle axes of periclase, when aligned in flow, are rotated about the vertical by 45° (Fig. 9). For columbite the principle axes are rotated in the vertical plane by 135°. Hence, the SKS and SKKS phases pass through the principle axes at different azimuths, about 47° (SKS) and 69° (SKKS), respectively (Fig. 10).

The transmission coefficients of the tubules (Figs. 4 and 5) and disks (Figs. 6 and 7) are similar even though the models initially appear to be very different. This is because both models have hexagonal symmetry with the symmetry axis along x_1. For the tubules, the

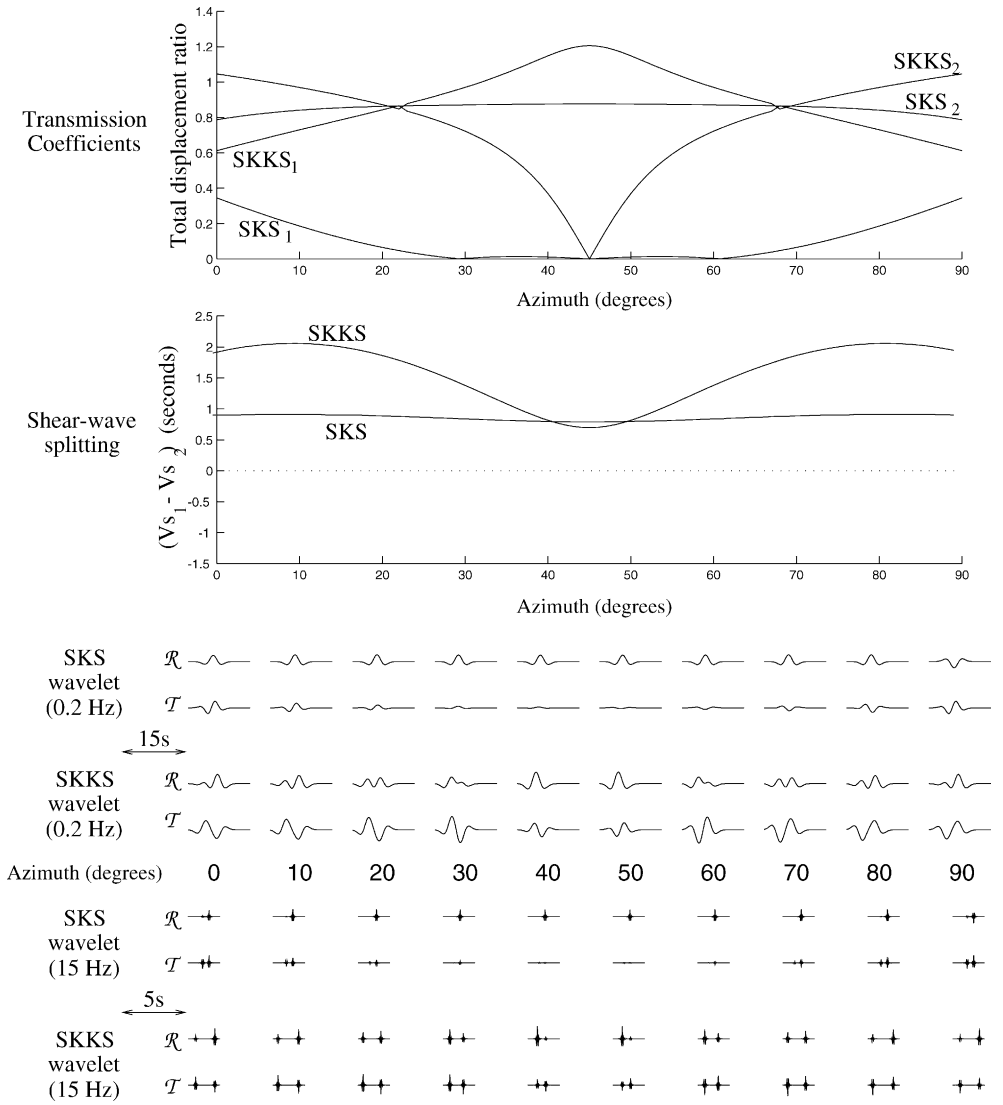

Fig. 9. D″ anisotropy due to partially aligned periclase. Results are for SKS and SKKS phases at an epicentral distance of 110°. The figure (from top to bottom) shows azimuthal variations in transmission coefficients at the CMB, shear-wave splitting times, and the resulting radial (R) and transverse (T) component waveforms with 0.2 Hz and 15 Hz dominant frequencies. A time window of 15 s is shown for the 0.2 Hz waveforms and a shorter time window of 3 s is shown for the 15 Hz waveforms.

isotropy plane, x_2–x_3, is a plane of slow P-waves and for the disks this is a plane of faster P-wave velocities. The perovskite model shows similar transmission coefficients (Fig. 8). Although strictly speaking perovskite has orthorhombic symmetry, it can be nearly approximated as also having hexagonal symmetry. The other LPO models on the other hand display quite different azimuthal variations since their symmetry is quite different from hexagonal: columbite is orthorhombic (Fig. 10), and periclase is cubic (Fig. 9).

The second row in Figs. 4–10 displays the predicted shear-wave splitting for all 7 models and the lower part the numerical waveforms for 0.2 Hz and 15 Hz, respectively. Again, azimuth-dependent variations in shear-wave splitting are clearly visible except for the tubule-inclusion models (Figs. 4 and 5).

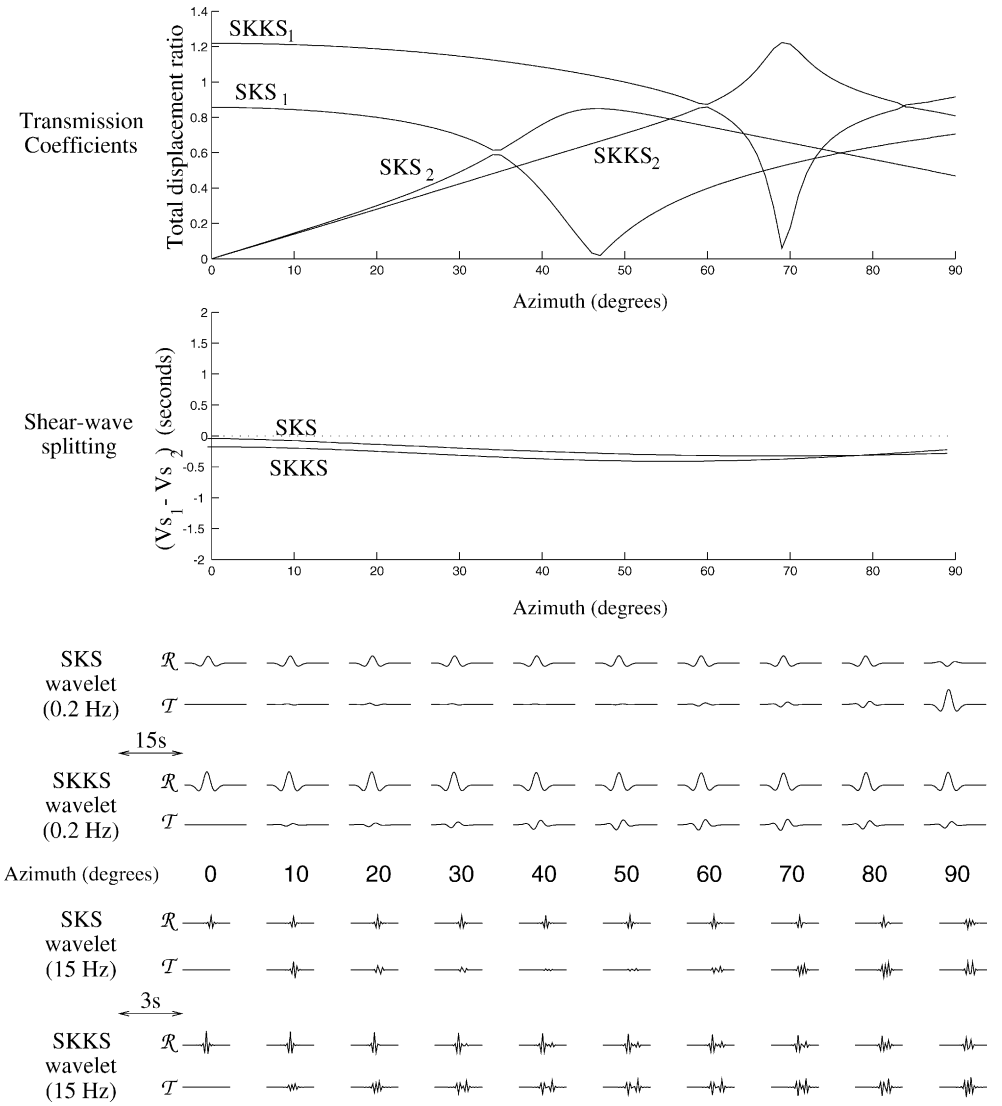

Fig. 10. D″ anisotropy due to partially aligned columbite. Results are for SKS and SKKS phases at an epicentral distance of 110°. The figure (from top to bottom) shows azimuthal variations in transmission coefficients at the CMB, shear-wave splitting times, and the resulting radial (R) and transverse (T) component waveforms with 0.2 Hz and 15 Hz dominant frequencies. A time window of 15 s is shown for the 0.2 Hz waveforms and a shorter time window of 3 s is shown for the 15 Hz waveforms.

These variations show that the maximum splitting may be observed near to one of the principle axes. However, along these axes, only one shear-wave is produced since the transmission coefficient is zero for the other shear wave (upper row in Figs. 4–10). Hence, a null measurement would result at these particular azimuths. This can also be seen in the synthetic waveforms (lower rows).

For aligned disk-shaped inclusions (Figs. 6 and 7), the shear-wave group-velocity surfaces cross at particular phase angles. This results in zero shear-wave splitting at these shear-wave intersection singularities and the polarity of the leading shear-wave will be orthogonal on either side of the intersection (Crampin and Yedlin, 1981). It is interesting that in our case this singularity only affects the SKKS phase and not SKS. The

SKS phase does not pass through the shear-wave intersection singularity due to its more vertical incidence angle at the CMB. As the SKKS phase passes through the singularity, a change in polarity of the waves is observed in both the 15 Hz and 0.2 Hz wavelets around 45° and 35° for the melt and solid inclusions, respectively. It should be noted that our ray-based modelling of the waveforms does not account for any coupling between the two shear-waves near this singularity (Chapman and Shearer, 1989), but as these models are laterally continuous and the anisotropy is homogeneous there should not be any coupling.

In each model the transmission coefficients also show azimuths where the relative strength of the two shear-waves changes sign. Near these azimuths the energy on the transverse component of the 15 Hz waveforms can get quite large. However, with the longer-period and more realistic 0.2 Hz waveforms there are constructive and destructive interference effects between the fast and slow shear-waves. As a consequence, in most cases the radial component displays large amplitudes due to constructive interference and the transverse component shows smaller amplitudes due to destructive interference. The exceptions are SKKS at most azimuths in the periclase model (Fig. 9) and SKS very near azimuths of 90° in the columbite model (Fig. 10). These are the two models that are not hexagonal in their anisotropic symmetry.

4. Conclusions

Our modelling suggests that SKS and SKKS splitting accrued in the D″ region can be significant. However, the nature of the splitting is not always intuitive. A VTI mantle will not generate any SKS or SKKS splitting due to the nature of the P-to-S conversion at the CMB. Only azimuthal anisotropy will cause SKS and SKKS splitting. In terms of SPO anisotropy, oriented low-velocity inclusions are much more effective in generating shear-wave splitting than high-velocity inclusions. Horizontally-aligned tubule-shaped inclusions produce small amounts of splitting, little azimuthal variation in splitting and similar SKS and SKKS splitting. Vertically-aligned disk-shaped inclusions are more effective at generating splitting. This model shows strong azimuthal variations in splitting with clear discrepancies between SKS and SKKS. Aligned perovskite produces small amounts of splitting, with little azimuthal dependence and little discrepancies between SKS and SKKS. In contrast, aligned periclase produces large amounts of splitting, large azimuthal variations in SKKS splitting, but not SKS splitting, and significant discrepancies in SKKS and SKS splitting. Aligned columbite produces little splitting, but significant azimuthal variations in the strength of the transmitted waves. Columbite is strongly anisotropic, but because it has such high seismic velocities it cannot occur in quantities large enough to produce appreciable splitting and still be compatible with data-derived seismic models.

Results were presented for SKS and SKKS waveforms at an epicentral distance of 110°. Shear-wave splitting measurements can be made for both phases only over a limited range of distances, ∼100–120°. The incidence angles at the CMB for these phases varies by less than 10° over this range. We therefore do not expect significant variations in the results over the limited range of distances where both SKS and SKKS can be observed.

It is important to note that all models, including VTI models, would produce appreciable shear-wave splitting in phases which turn or reflect in the lower mantle (e.g., S at distances beyond 90°). It is difficult to predict how these models will affect waveforms of phases like ScS, S and Sdiff. Simple ray theory is not appropriate for modelling such waveforms in an anisotropic D″ model. Complications due to waveform coupling, travel-time triplications and coupling with the liquid outer core make this a more challenging problem. Maupin (1994) has shown, for example, how complicated Sdiff phases can be in a VTI D″ layer.

In summary, most of the mechanisms for D″ anisotropy considered here produce small amounts of SKS and SKKS splitting, on the order of that produced by the crust (<0.5 s). The exceptions are vertically-aligned disk-shaped melt-filled inclusions and aligned periclase. Splitting due to these two mechanisms could significantly mask the effects of upper-mantle anisotropy. Diagnostics for these styles of lower-mantle anisotropy are strong azimuthal variations in splitting and discrepancies between SKS and SKKS splitting. However, assessing azimuthal variations in splitting for a particular region of lower mantle is difficult due to the sparsity of earthquakes and receivers. Discrepancies between SKS and SKKS

splitting, as observed, by James and Assumpção (1996), provide more hope. Nevertheless, the effects of CMB topography (Restivo et al., 1998) and lateral variations in mantle velocity-structure should also be considered when interpreting SKS and SKKS discrepancies.

Our modelling provides a means for assessing the effects of mantle anisotropy on a range of phases. New models can be tested as our knowledge of the elasticity and deformation mechanisms for deep mantle minerals improves.

Acknowledgements

We thank two anonymous reviewers for their helpful suggestions and we thank the editor, Dave Gubbins, for his help with this paper and his many years of editing PEPI.

References

Aki, K., Richards, P.G., 1980. Quantitative Seismology: Theory and Methods. Freeman Press, San Francisco, USA, 992 pp.

Anderson, O.L., 1965. Determination and some uses of isotropic elastic constants of polcrystalline aggregates using single crystal data, in: Mason, P.M. (Ed.), Physical Acoustics, 3B, pp. 43–95.

Chapman, C.H., Shearer, P.M., 1989. Ray tracing in azimuthally anisotropic media-II. Quasi-shear wave coupling. Geophys. J. Int. 96, 65–83.

Crampin, S., Yedlin, M., 1981. Shear-wave singularities of wave propagation in anisotropic media, A review of wave motion in anisotropic and cracked elastic media. J. Geophys. 49, 43–46.

Dziewonski, A.M., Anderson, D.L., 1981. Preliminary reference earth model. Phys. Earth Planet. Int. 25, 297–356.

Guest, W.S., Kendall, J.-M., 1993. Modelling seismic waveforms in anisotropic inhomogeneous media using ray and Maslov asymptotic theory: applications to exploration seismology. Can. J. Expl. Geophys. 29, 78–92.

Hill, R., 1952. The elastic behaviour of a crystalline aggregate. Proc. Phys. Soc. (Lond.) A65, 349.

James, D.E., Assumpção, M., 1996. Tectonic implications of S-wave anisotropy beneath SE Brazil. Geophys. J. Int. 126, 1–10.

Karato, S., 1998. Some remarks on the origin of seismic anisotropy in the D″ layer. Earth Planets Space 50, 1019–1028.

Kendall, J.-M., Silver, P.G., 1998. Investigating causes of D″ anisotropy, in: Gurnis, M., Wysession, M., Knittle, E., Buffet, B. (Eds.), Core–Mantle Boundary Region, Geodynamic Series, vol. 28. American Geophysical Union, Washington, DC, USA, pp. 97–118.

Lay, T., Garnero, E.J., Williams, Q., Romanowicz, B., Kellogg, L., Wysession, M.E., 1998. Seismic wave anisotropy in the D″ region and its implications, in: Gurnis, M., Wysession, M., Knittle, E., Buffet, B. (Eds.), Core–Mantle Boundary Region, Geodynamic Series, vol. 28. American Geophysical Union, Washington, DC, USA, pp. 229–318.

Mallick, S., Frazer, L.N., 1991. Reflection–transmission coefficients and azimuthal anisotropy in marine seismic studies. Geophys. J. Int. 105, 241–252.

Maupin, V., 1994. On the possibility of anisotropy in the D″ layer as inferred from the polarization of diffracted S-waves. Phys. Earth Planet. Int. 87, 1–32.

Oganov, A.R., Brodholt, J.P., Price, G.D., 2001. The elastic constants of $MgSiO_3$ perovskite at pressures and temperatures of the Earth's mantle. Nature 411, 934–937.

Restivo, A., Helffrich, G., Kendall, J.-M., 1998. core–mantle boundary heterogeneities inferred from anomalous SKS and SKKS splitting. EOS: Trans. Am. Geophys. Un. 79, F617.

Savage, M., 1999. Seismic anisotropy and mantle deformation: what have we learned from shear wave splitting. Revs. Geophys. 37, 65–106.

Silver, P.G., 1996. Seismic anisotropy beneath the continents: probing the depths of geology. Ann. Rev. Earth Space Sci. 24, 385.

Stixrude, L., 1998. Elastic constants and anisotropy of $MgSiO_3$ perovskite, periclase and SiO_2 at high pressure, in: Gurnis, M., Wysession, M., Knittle, E., Buffet, B. (Eds.), Core–Mantle Boundary Region, Geodynamic Series, vol. 28. American Geophysical Union, Washington, DC, USA, pp. 83–96.

Tandon, G.P., Weng, G.J., 1984. The effect of aspect ratio of inclusions on the elastic properties of unidirectionally aligned composites. Polym. Compos. 5, 327–333.

Yamazaki, D., Karato, S.-I., 2002. Fabric development in (Mg,Fe)O during large strain, shear deformation; implications for seismic anisotropy in Earth's lower mantle. Phys. Earth Planet. Int. 131, 251–267.